Chemical Geology 492 (2018) 12–19

Contents lists available at ScienceDirect

Chemical Geology

journal homepage: www.elsevier.com/locate/chemgeo

Effect of Zn(II) coprecipitation on Mn(II)-induced reductive transformation of birnessite

Shiliang Zhao[a], Yaneira A. González-Valle[a], Evert J. Elzinga[b], Emily M. Saad[a], Yuanzhi Tang[a,*]

[a] School of Earth and Atmospheric Sciences, Georgia Institute of Technology, Atlanta, GA 30332-0340, USA
[b] Department of Earth & Environmental Sciences, Rutgers University, Newark, NJ 07102, USA

ARTICLE INFO

Editor: Dong Hailiang

Keywords:
Manganese oxide
Birnessite
Zinc
Coprecipitation
Transformation

ABSTRACT

Mn oxides (MnOx) are ubiquitous metal oxide minerals in nearly all environmental settings. They play important roles in the transport and fate of many environmental components such as metals, organics, and nutrients. In the presence of dissolved Mn(II), MnOx phases can undergo ripening and transformation, resulting in the formation of phases with higher structural order, thus strongly affect the reactivity of MnOx over extended time scale. In natural environments, metal cations can strongly interact with MnOx through mechanisms such as sorption, incorporation, and/or coprecipitation, yet much still remain unknown about the effect of metal coprecipitation on the transformation of MnOx. This study investigates the effects of Zn coprecipitation on Mn(II)-induced reductive transformation of birnessite, a common MnOx mineral phase. Pure and Zn-coprecipitated acid birnessite phases were synthesized and their transformation kinetics and pathways in the presence of Mn(II) was investigated under oxic or anoxic conditions. During the transformation process, Zn-coprecipitated birnessite showed higher capability toward Mn(II) uptake, likely due to smaller particle size and the fast consumption of Mn(II) and precipitation of a new phase hetaerolite. The formation of an intermediate phase, feitknechtite, was faster for Zn-coprecipitated birnessite than pure birnessite, which is the opposite of Zn-sorbed birnessite system. Transformation from the intermediate phase feitknechtite to the final stable phase manganite was slower for Zn-coprecipitated birnessite, due to the lower Mn(II) concentration which catalyzed the transformation. This study revealed the importance of understanding the influence of metal cation impurities on the structural stability and long term reactivity of Mn oxide minerals.

1. Introduction

Mn oxides (MnOx) are ubiquitous metal oxide minerals in nearly all environmental settings, such as fresh waters, marine nodules, soils, and sediments (Bodeï et al., 2007; Bargar et al., 2009; Lanson et al., 2008). They are generally produced through the oxidation of Mn(II), and this process is much faster when catalyzed by mineral surfaces, microorganisms (Tebo et al., 2004), or reactive oxygen species (ROS) (Learman et al., 2011; Jung et al., 2017a, 2017b). Microorganisms are highly effective in catalyzing MnOx production (Learman et al., 2011; Jung et al., 2017a, 2017b; Murray et al., 2007; Bargar et al., 2005), and the initial biogenic MnOx are typically highly reactive hexagonal phases with high surface area, negative surface charge, and large amount of vacancy sites (Tebo et al., 2004). Dissolved Mn(II) can react with structural Mn(IV) to produce Mn(III) (Bargar et al., 2005; Zhu et al., 2010; Tang et al., 2014; Zhao et al., 2016), resulting in the ripening and transformation of the hexagonal birnessite phases and the formation of phases with different symmetry (i.e. triclinic birnessite) or oxidation states (i.e. Mn(III)-bearing oxides and hydroxides) (Webb et al., 2005; Post, 1999). Such reductive transformation can strongly affect the sorptive and redox reactivity of the MnOx. For example, newly produced Mn(III) can incorporate at the vacancy sites of MnOx and decrease the sorption capacity toward metal cations (e.g. Pb, Cu, Zn, and Cd) (Wang et al., 2012). Mn(III)-bearing minerals are less reactive compared to Mn(IV)-bearing minerals toward the adsorption of As(III, V) (Zhu et al., 2009). The availability of Mn(III) in MnOx structure is also important during the oxidation of Cr(III) by MnOx (Landrot et al., 2012; Nico and Zasoski, 2000).

The reductive transformation process is controlled by factors such as dissolved Mn(II) concentration, pH, and the presence of oxygen (O_2). At low Mn(II) concentrations, biotic and abiotic hexagonal birnessite can react with Mn(II) to form Mn(III), which can order within the layer and change the layer symmetry from hexagonal to triclinic (Bargar et al., 2005; Zhu et al., 2010; Zhao et al., 2016). With higher Mn(II) concentration and under anoxic conditions, such reductive transformation can lead to the formation of manganite (γ-MnOOH) at pH 7.0–8.0 and

* Corresponding author.
E-mail address: yuanzhi.tang@eas.gatech.edu (Y. Tang).

https://doi.org/10.1016/j.chemgeo.2018.05.031
Received 4 March 2018; Received in revised form 15 May 2018; Accepted 22 May 2018
Available online 23 May 2018
0009-2541/

hausmannite ($Mn^{II}Mn_2^{III}O_4$) at pH 8.0–8.5, both with the presence of an intermediate phase feitknechtite (β-MnOOH) (Elzinga, 2011; Lefkowitz et al., 2013). Under oxic conditions, hexagonal birnessite can react with concentrated Mn(II) and precipitate nsutite (γ-$Mn^{III,IV}(O,OH)_2$) and ramsdellite (MnO_2) at pH 2.4, cryptomelane ($K_{1.3–1.5}Mn_8^{III,IV}O_{16}$) at pH 4.0, groutite (α-MnOOH) at pH 6.0, and feitknechtite and manganite at pH 7–7.5 (Tu et al., 1994; Mandernack et al., 1995). The presence of oxygen generally increases the uptake of Mn(II) by birnessite, due to mineral-surface catalyzed oxidation of Mn(II) by O_2 in addition to the direct electron transfer reaction between Mn(II) and birnessite (Elzinga, 2011; Lefkowitz et al., 2013).

Birnessite minerals have high affinities for metal cations due to their low point of zero charge (PZC) (Tebo et al., 2004; Spiro et al., 2009) and negatively charged surface across a wide range of pH conditions. Adsorbed and/or incorporated metal impurities in birnessite are likely to affect the above-mentioned transformation processes. A few studies have examined the effects of metal sorption and/or presence on the reductive transformation process. Ni adsorption on biogenic birnessite (Zhu et al., 2010) was shown to inhibit the formation of Mn(III) and favor the hexagonal symmetry; whereas Na and Ca presence during the transformation of biogenic MnOx can stabilize layer Mn(III) and favor the triclinic symmetry (Zhu et al., 2010). Zn adsorption on birnessite was found to slow down the transformation from birnessite to feitknechtite under anoxic condition (Lefkowitz and Elzinga, 2015).

Coprecipitation of metal cations (e.g. Ni, Zn, Fe, and Co) is known to modify birnessite structural properties (e.g. average oxidation state, surface area, vacancy site density) (Yin et al., 2015a, 2013, 2014, 2012, 2011). For example, Zn coprecipitation with fungal MnOx was shown to interrupt layer stacking and result in thinner flake-shaped particles (Yu et al., 2013). Our recent study also showed that Zn coprecipitation with abiotic phyllomanganates (δ-MnO_2 and birnessite) resulted in reduced layer stacking and/or lateral layer size (Zhao and Wang, n.d.). Such effects, though previously observed for Zn adsorption on MnOx (Grangeon et al., 2012), were not as significant as the Zn coprecipitation system (Zhao and Wang, n.d.). Yet, despite the commonly observed structural modifications induced by metal coprecipitation with MnOx and the obvious environmental relevance, no studies have investigated how the structural modifications caused by metal coprecipitation would influence the long-term reductive transformation processes of MnOx.

In this study, we systematically compared the Mn(II)-induced transformation kinetics and pathways of pure and Zn-coprecipitated birnessite, and compared the effects to a previous study on the transformation of Zn-adsorbed birnessite (Lefkowitz and Elzinga, 2015). The roles of light and oxygen were also investigated by conducting experiments under light vs. dark conditions and oxic vs. anoxic conditions. To our knowledge, this is also the first study on the effects of Zn-birnessite interaction on birnessite reductive transformation under oxic conditions. Results from this study can help understand how metal impurities affect the long-term stability and reactivity of Mn oxides, thus Mn geochemical cycling in natural environments. For example, the formation of intermediate Zn-containing MnOx mineral phases as well as the overall transformation kinetics and pathways might significantly affect the sorptive and redox activities of the MnOx phases over extended time, and might also affect microbial anaerobic respiration of these oxides depending on the redox reactivity of the products.

2. Methods

2.1. Synthesis of pure and Zn-coprecipitated acid birnessite

Acid birnessite was synthesized following a previous study (Villalobos et al., 2003) by adding 45 mL of 6 M HCl to a boiling 300 mL of 0.667 M $KMnO_4$ solution under vigorous stirring. For Zn-coprecipitated birnessite samples, calculated amount of $ZnSO_4$ was mixed with the HCl solution before the addition of $KMnO_4$, to achieve $Zn:Mn_{total}$ molar ratio of 0.01, 0.1, and 0.2. These samples are labeled as 0.01 cppt, 0.1 cppt, and 0.2 cppt birnessite, respectively. At the end of reaction, the suspension was allowed cooling down and settling. The brown precipitates were collected by vacuum filtration (0.2 μm), washed and dialyzed with deionized (DI) water, and freeze dried. A portion of the solids were digested by aqua regia and measured for Zn and Mn concentrations using inductively coupled plasma–mass spectrometry (ICP-MS).

2.2. Mn(II)-induced transformation of birnessite phases

Parallel experiments were conducted to investigate the kinetics and pathways of Mn(II)-induced reductive transformation of pure and Zn-coprecipitated birnessite under oxic or anoxic conditions. For oxic experiments, 20 mg of pure or Zn-coprecipitated birnessite was suspended in a 200-mL solution containing 20 mM HEPES and 10 mM NaCl, with a solids/liquid ratio of 0.1 g/L. pH of the suspension was adjusted to 7.5 using NaOH and HCl solutions. The suspension was ultrasonicated for 3 min and equilibrated for 3 h by shaking at 150 rpm. To initiate the reaction, 200 μL of 1 M $MnSO_4$ stock solution was added to the suspension to achieve 1 mM Mn(II) concentration. Reaction bottles were consistently agitated on an orbital shaker at 150 rpm for 18 days. At certain time point, aliquots of the reaction suspension were collected and vacuum-filtered (0.22 μm). Mn(II) concentration in the filtrate was determined using a colorimetric method (Madison et al., 2011) using a UV–vis spectrometer (Cary 60, Agilent). Zn concentration was analyzed using ICP-MS. Filtered solids were repeatedly rinsed with DI water and freeze-dried for later structural characterization. For anoxic experiments, all reactions were conducted inside a glove box (Coy) filled with 95% N_2 and 5% H_2. All solutions used for the experiments were boiled and cooled down under N_2 bubbling before transferring into the glove box. The transformation experiments above were conducted under dark conditions (bottles wrapped with aluminum foil). To investigate the potential influence of Mn oxide photo-reduction, the effect of light was also investigated using transparent plastic bottles under ambient lab lighting with other conditions same as above.

2.3. Solid phase characterization

A suite of complementary techniques were used to analyze the morphology and structure of the pure and Zn-coprecipitated birnessite, as well as their transformation products. X-ray diffraction (XRD) analysis was conducted using a Panalytical Empyrean multipurpose diffractometer with Cu Kα radiation and a PIXcel 3D-Medipi×3 1 × 1 detector. Freeze-dried samples were placed on a zero-background holder, and data collection was conducted at 0.03° 2θ interval with 4 s counting time per step. Fourier transformed infrared (FT-IR) spectroscopy analysis was conducted on a Bruker Vertex 80 V spectrometer using KBr pellets at 800–1250 cm^{-1}. FTIR spectra were normalized by the highest peak intensity in each spectrum, according to previous studies (Elzinga, 2011; Lefkowitz et al., 2013; Lefkowitz and Elzinga, 2015). High resolution transmission electron microscopy (HRTEM) analysis was conducted on a JEOL 2010F TEM. Solid samples were suspended in ethanol and ultrasonicated for 1 min, then a single drop of the suspension was added on a 200-mesh Cu grid with a holey-carbon support film and air dried. Image focus was obtained on the carbon film adjacent to the particles of interest to avoid beam damage, then the beam was moved to the sample for image collection.

For Mn and Zn K-edge XAS analysis, wet pastes of the synthesized birnessite samples were vacuum filtered using a 0.22 μm membrane, rinsed with DI water, and mounted in an acrylic sample holder covered with Kapton tape. Samples were stored at −20 °C before analysis. XAS experiments were conducted at Beamline 4-1 at Stanford Synchrotron Radiation Lightsource (SSRL, Menlo Park, CA) and beamlines 5-BM-D and 12-BM-B at Advanced Photon Source (APS; Argonne National Laboratory, Lemont, IL). Energy calibration used the corresponding Mn or Zn metal foil. Spectra of reference foils were collected

simultaneously with sample scans. XAS data were collected in both fluorescence and transmission mode at room temperature using a Vortex detector (APS 5-BM-D) or a 13 element Ge solid-state detector (APS 12-BM-B and SSRL 4-1). Both X-ray absorption near edge structure (XANES) and extended X-ray absorption fine structure (EXAFS) data were collected. Reference compounds (feitknechtite, manganite, pure and Zn-substituted hausmannite and hetaerolite) were from Lefkowitz and Elzinga (2015).

XAS data processing and analysis used the programs SIXpack (Webb et al., 2005) and Ifeffit (Ravel and Newville, 2005). Multiple scans (2–6) were energy calibrated and averaged for further analysis. Principal component analysis (PCA) was conducted on the normalized sample spectra to determine the number of components needed for obtaining reasonable fits. Using the corresponding reference compound spectra library, target transformation (TT) was conducted to determine appropriate candidate compounds. Linear combination fitting (LCF) was conducted on the EXAFS region. Combinations of TT-determined candidate compounds were used, and the goodness of fit was determined by R-factor. Fits with smallest R-factors were used.

3. Results and discussion

3.1. Effects of Zn-coprecipitation on birnessite properties

HRTEM images of pure and 0.2 cppt birnessite samples are presented in Fig. 1. Both samples contain low crystallinity particles with heavy aggregation, making it difficult to directly measure particle size. In general, thinner nano-sheets were observed in Zn-coprecipitated birnessite samples compared to pure birnessite sample. XRD patterns of the unreacted samples were shown in Fig. 2 (reaction t = 0). The peaks (001) and (002) at ~13° (labeled as "B") and 24° in pure birnessite sample can provide an overall estimation of the thickness of birnessite particles. With Zn coprecipitation, both peaks became lower and broader, indicating less layer stacking. A previous study also reported that Zn inhibited fungal Mn oxide growth and resulted in thinner particles (Yu et al., 2013). Grangeon et al. (2012) found that Zn sorption onto δ-MnO_2 caused mineral dissolution and smaller lateral coherent domain size. Zn might also cause smaller lateral layer size in the Zn-coprecipitated samples which requires more detailed XRD model fitting as described in previous studies (Grangeon et al., 2012). Coprecipitation of other heavy metals (e.g. Ni, Co, Cu, and Fe) has also been previously shown to influence the crystallization of abiotic (Yin et al., 2013, 2012, 2011; Grangeon et al., 2012) and biotic (Yu et al., 2013) birnessite, producing birnessite particles with less stacking layers and/or smaller lateral layer dimension, i.e., overall smaller particle size.

Both pure and Zn birnessite solids were analyzed by digestion and ICP-MS to obtain the Zn and total Mn contents (Table 1). Mn content barely changed by Zn coprecipitation, while K content was significantly reduced. Interestingly, the reduced K content (~0.23 mM) was almost twice of the structural Zn (~0.12 mM), which is expected for a direct cation exchange mechanism that maintains the same interlayer charge. Previous studies showed that adsorbed (Lanson et al., 2002; Manceau et al., 2002; Kwon et al., 2013) or coprecipitated (Yu et al., 2013) Zn did not substitute for Mn atoms in the layer, but was adsorbed above or below the layer vacancy sites, replacing interlayer K (Lanson et al., 2002), and have minimum effects on Mn contents. With the same birnessite concentration (0.1 g/L) in both pure and Zn coprecipitated systems, total Mn content in the solids were almost the same.

3.2. Transformation of pure birnessite under anoxic condition

When Mn(II) reacted with pure birnessite under anoxic condition, Mn(II) can instantly sorb onto birnessite vacancy sites at interlayer and edge regions, replacing other previously sorbed cations (e.g. Zn^{2+}) before further reactions occur (Elzinga, 2011; Lefkowitz and Elzinga, 2015; Villalobos et al., 2014). This is consistent with the observed fast decrease of Mn(II) concentration after adding Mn(II) to both pure and Zn-coprecipitated birnessite systems (Fig. 3A). Fig. 2 shows the XRD data of solid products during the 18-day transformation process. After Mn(II) addition, peak B decreased along with the growth of other peaks, indicating that adsorbed Mn(II) reacted with birnessite and produced new mineral phases. Previous study also found that HEPES buffer can cause partial dissolution of birnessite and production of Mn(II) (Elzinga and Kustka, 2015). After comparison with XRD spectra of reference compounds (details in Text S1 and Fig. S1), the growing peaks belong to feitknechtite (β-MnOOH), which indicates electron transfer from Mn(II) to structural Mn(IV), producing Mn(III)-containing mineral phase (Eq. (1)), consistent with the results of previous studies (Elzinga, 2011; Lefkowitz et al., 2013; Lefkowitz and Elzinga, 2015). The two bands at 1067 and 946 cm^{-1} in FT-IR spectra (Fig. 4), resulting from OH bending, (Elzinga, 2011; Lefkowitz et al., 2013; Lefkowitz and Elzinga, 2015) confirm the existence of feitknechtite. Feitknechtite production likely continuously decreased Mn(II) concentration in the following 5 days under anoxic condition.

$$Mn^{2+}_{(aq)} + MnO_{2(s)} + 2H_2O \rightarrow 2\beta\text{-}MnOOH_{(s)} + 2H^{+}_{(aq)} \quad (1)$$

Mn(II) concentration reached a steady state after 5 days and stay unchanged (~0.44 mM) in the next 13 days. Peak "F" gradually disappeared with the growth of new peaks such as the peak "M" at ~29°. These new peaks belong to a more stable Mn(III)-containing phase manganite (γ-MnOOH, Eq. (2)). Three appearing bands at 1150, 1116, and 1087 cm^{-1} in FT-IR data (Elzinga, 2011; Lefkowitz et al., 2013;

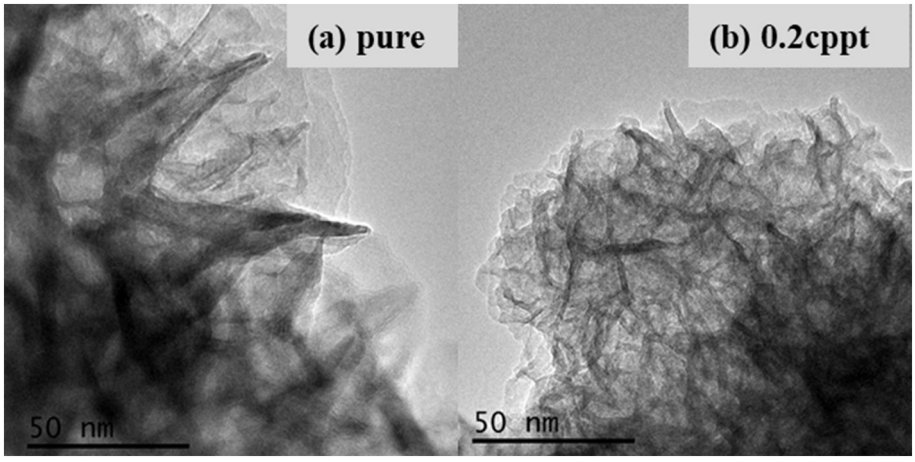

Fig. 1. HRTEM images of pure and Zn-coprecipitated birnessite samples.

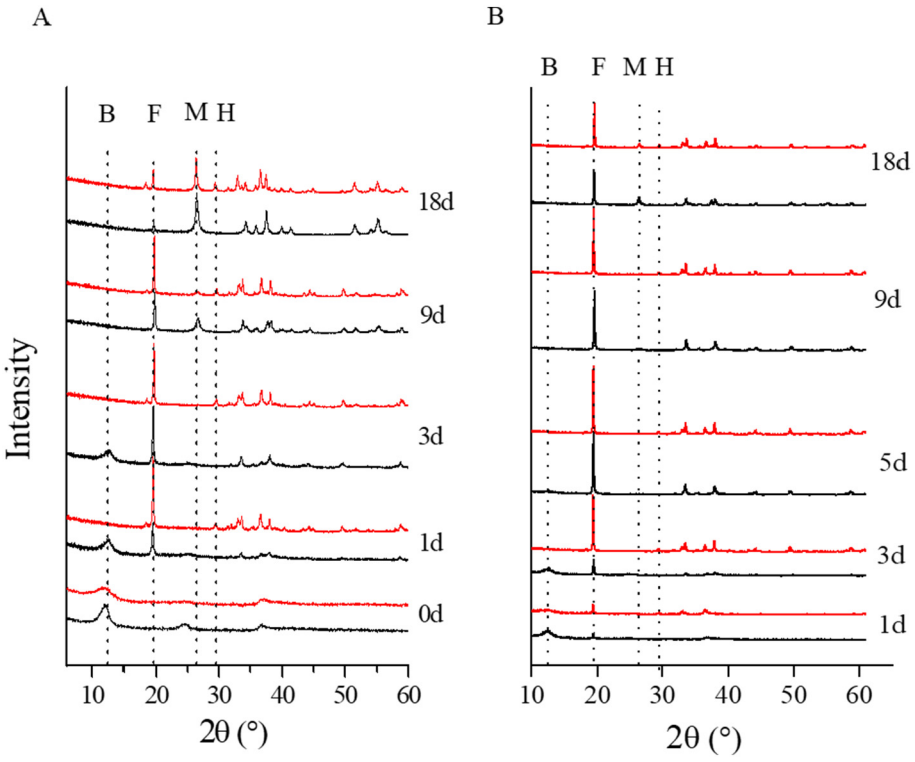

Fig. 2. XRD spectra of pure (black) and 0.2_cppt Zn-coprecipitated birnessite (red) samples after reaction under (a) anoxic or (b) oxic conditions at pH 7.5 for 18 d. "B", "F", "M" and "H" indicate the peak positions for birnessite, feitknechtite, manganite, and hetaerolite, respectively. (For interpretation of the references to color in this figure legend, the reader is referred to the web version of this article.)

Table 1
Concentrations of dissolved Mn(II) in the reaction solution (measured by colorimetric method), as well as the concentrations of total Mn in birnessite, Zn, and K (measured by ICP-MS) in pure or Zn-coprecipitated birnessite samples before and after 18 d reaction under anoxic or oxic conditions. To better compare with dissolved Mn(II) concentration, concentrations of total Mn, Zn, and K in birnessite were converted to mM by normalizing the contents by total liquid volume.

Reaction condition	Birnessite phase	$[Mn(II)]_{aq}$ (mM)		[Mn] in birnessite (mM)		[Zn] in birnessite (mM)	[K] in birnessite (mM)
		t = 0	t = 18 d	t = 0	t = 18 d[a]		
Anoxic	Pure	1.0	0.44	0.76	0.20	0	0.27
	0.2 cppt	1.0	0.26	0.72	0	0.12	0.04
Oxic	Pure	1.0	0.09	0.76	–	0	0.27
	0.2 cppt	1.0	0.11	0.72	–	0.12	0.04

[a] The total Mn remaining in birnessite at day 18 was calculated according to dissolved Mn(II) concentration and Eq. (1).

Lefkowitz and Elzinga, 2015) confirmed the transformation from feitknechtite to manganite (Elzinga, 2011; Lefkowitz et al., 2013; Lefkowitz and Elzinga, 2015). This process does not consume Mn(II), resulting in a sustained Mn(II) concentration from day 5 to 18. The ratio between initial Mn(II) (1 mM) and Mn(IV) concentrations (0.76 mM) is larger than the 1:1 Mn(II)/Mn(IV) stoichiometry in Eq. (1), but ~0.20 mM Mn(IV) remained in the solids after 18-day reaction (Table 1). This is probably due to the newly formed Mn-bearing phases preventing the further reaction between birnessite and Mn(II).

$$\beta\text{-MnOOH}_{(s)} \rightarrow \gamma\text{-MnOOH}_{(s)} \quad (2)$$

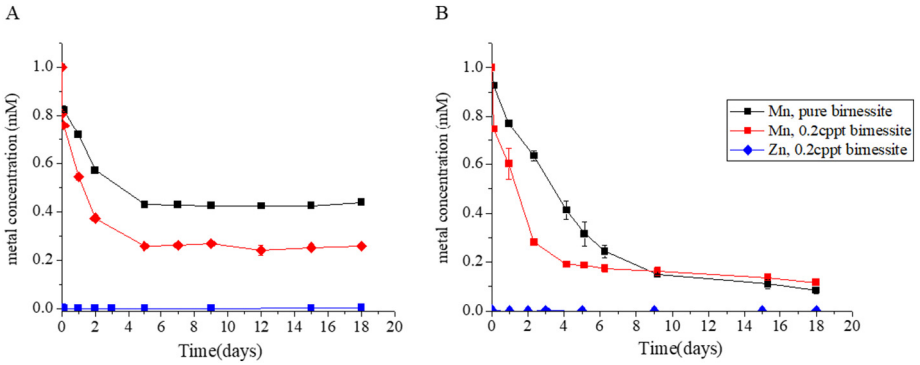

Fig. 3. Concentrations of dissolved Mn(II) and Zn(II) in the reaction suspension during the reductive transformation of pure or 0.2 cppt-birnessite under (A) anoxic and (B) oxic conditions at pH 7.5.

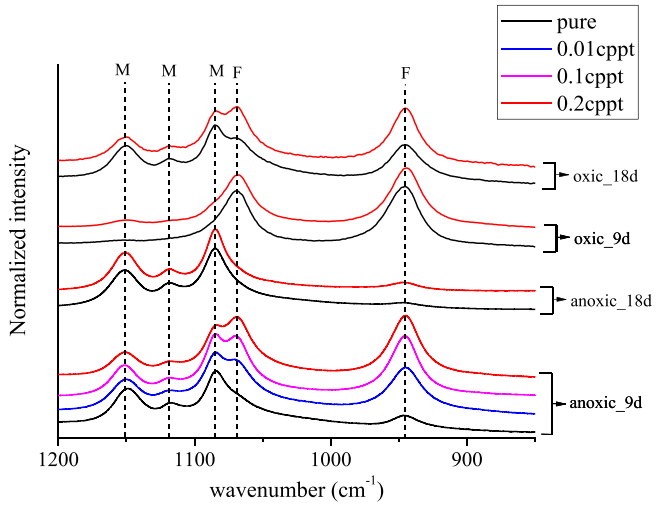

Fig. 4. FTIR spectra of pure and Zn-coprecipitated birnessite samples after reaction under anoxicor oxic conditions at pH 7.5. "F" and "M" stand for feitknechtite and manganite.

3.3. Transformation of pure birnessite under oxic condition

Under oxic conditions, Mn(II) concentration quickly decreased during the first few days, similar to the observed trend under anoxic condition (Fig. 3B). This fast decrease was mostly attributed to Mn(II) adsorption and reaction with birnessite. Mn(II) concentration continuously decreased, compared to reaching a steady state concentration under anoxic condition. The continuous removal of Mn(II) from the solution was likely due to surface-catalyzed oxidation of Mn(II) by oxygen under oxic conditions (Eq. (3)) (Elzinga, 2011; Lefkowitz et al., 2013; Lefkowitz and Elzinga, 2015). Mn(II) oxidation by oxygen is kinetically slow at neutral pH (Tebo et al., 2004), but can become faster when catalyzed by Mn-oxide mineral surfaces (i.e., birnessite and feitknechtite in this study) (Lefkowitz et al., 2013). At day 9, both the XRD patterns (Fig. 2) and the normalized FT-IR spectra (Fig. 4) showed a higher content of feitknechtite but little manganite under oxic condition, as compared to the results under anoxic condition. At day 18, a significant amount of feitknechtite remained in the oxic system, whereas nearly all feitknechtite were transformed to manganite at day 9 under anoxic condition. This is because feitknechtite was produced through Mn(II) oxidation by both birnessite (i.e. direct oxidation) and oxygen (i.e. mineral catalyzed oxidation) in the oxic system, whereas Mn(II) oxidation was only through birnessite (direct oxidation) in the anoxic system (Elzinga, 2011; Lefkowitz et al., 2013; Lefkowitz and Elzinga, 2015).Under oxic condition, feitknechtite was continuously produced in the presence of both oxygen and mineral surfaces throughout 18 days, whereas under anoxic condition the production stopped at ~day 5. In addition, the transformation from feitknechtite to manganite was also catalyzed by Mn(II). Low Mn(II) concentration (after day 5) might have accounted for the slow transformation of feitknechtite to manganite under oxic condition.

$$4Mn^{2+}_{(aq)} + O_{2(aq)} + 6H_2O \rightarrow 4\beta\text{-}MnOOH_{(s)} + 8H^{+}_{(aq)} \quad (3)$$

3.4. Transformation of Zn-coprecipitated birnessite under oxic and anoxic conditions

Parallel experiments were conducted on pure and Zn-coprecipitated birnessite under oxic vs. anoxic and light vs. dark conditions. Under light vs. dark conditions, no significant difference was observed in Mn (II) concentration (Fig. S3) and solid phase structure (Fig. S4). Under oxic vs. anoxic conditions, the effects of Zn-coprecipitation on the transformation process had similar trends, as discussed below.

3.4.1. Hetaerolite precipitation

Based on XRD data in Fig. 2 (t = 0), Zn-coprecipitation did not cause the formation of additional phases other than birnessite. The k^3-weighted Zn EXAFS data and Fourier transformed spectra of 0.2_cppt birnessite sample are shown in Fig. 5. Shell-by-shell fitting results in our recent study (Zhao and Wang, n.d.) showed that Zn mostly existed in octahedral configuration and as surface adsorbed species. In previous studies (Lefkowitz and Elzinga, 2015; Hinkle et al., 2017), it was shown that Zn(II) and Mn(II) can strongly compete with each other during adsorption. Pre-adsorbed Zn(II) can decrease birnessite sorption capacity toward Mn(II) at pH 6 (Lefkowitz and Elzinga, 2015). At low Mn(II) loading, Mn(II) can replace pre-adsorbed Zn(II) on birnessite and δ-MnO_2 vacancy sites at pH 4 (Hinkle et al., 2017). However, in this study with high Mn(II) concentration (1 mM) and higher reaction pH (7.5), no desorbed aqueous Zn was observed in both anoxic and oxic systems throughout the 18-day reaction, even within the first few minutes (Fig. 3). On the other hand, compared to pure birnessite system, Zn-coprecipitated birnessite showed a much higher Mn(II) sequestration rate under both anoxic and oxic conditions. Under anoxic condition, a lower steady state Mn(II) concentration was reached after 5 days. Because Zn-coprecipitation produced birnessite phases with smaller particle size, the subsequent increase in surface area might have contributed (at least partially) to the faster Mn(II) uptake as compared to the pure birnessite system.

Besides feitknechtite and manganite, XRD data of Zn-coprecipitated birnessite samples showed additional peaks at ~18°, 29°, and 33° (Figs. S1 and S3). These peaks correspond to a new phase hetaerolite ($ZnMn^{III}_2O_4$), formed by Zn coprecipitation with newly produced Mn (III), as shown in Eq. (4). Hetaerolite production was previously observed in systems involving Zn and Mn redox reactions (Lefkowitz and

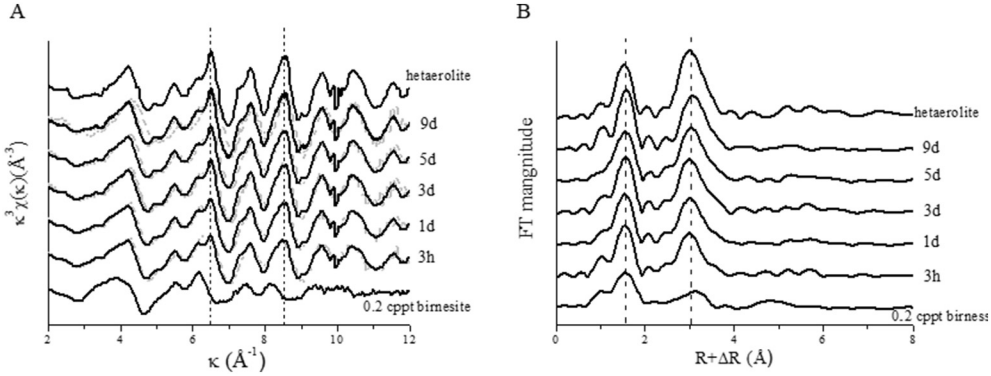

Fig. 5. k^3-weighted Zn EXAFS (A) and Fourier transformed (B) spectra (not corrected for phase shift) of 0.2 cppt birnessite anoxic transformation products. Raw and fitted data are in solid and dotted lines, respectively.

Elzinga, 2015; Chang et al., 2014). The precipitation of hetaerolite also consumed Mn(II) and Mn(IV) at a 1:1 ratio, same as feitknechtite production in Eq. (1). Based on mass balance calculation (Table 1), the reaction in pure systems was not complete. Both Mn(IV) and Mn(II) remained at stable stage. In comparison, nearly all Mn(IV) in Zn-coprecipitated birnessite was consumed after 18 days. Mn(III) in solutions readily undergoes disproportionation into Mn(II) and Mn(IV) (Tebo et al., 2004; Zhu et al., 2010; Murray et al., 1985). The precipitation of feitknechtite and hetaerolite in this study removed Mn(III) from solutions and preserved it. Previous study showed that hetaerolite acted as a stronger sink of Mn(III) compared to feitknechtite (Lefkowitz and Elzinga, 2015), consistent with the complete consumption of Mn(II) and Mn(IV) in the anoxic Zn systems. The rapid precipitation of hetaerolite relative to feitknechtite may be another cause of the faster Mn(II) uptake by Zn coprecipitated birnessite.

$$Mn^{2+}_{(aq)} + MnO_{2(s)} + Zn^{2+}_{(aq)} + 2H_2O \rightarrow ZnMn^{III}{}_2O_{4(s)} + 4H^+_{(aq)} \quad (4)$$

Fig. 5 shows the k^3-weighted Zn EXAFS data and Fourier transformed spectra of initial Zn-coprecipitated birnessite and the transformation products under anoxic condition. Pure hetaerolite was also plotted as a reference compound. Zn-coprecipitated birnessite and hetaerolite showed distinct features at 6–12 Å in k space, especially the peaks at ~6.5 and 8.5 Å. The evolution of both peaks suggested the gradual transformation from surface adsorbed Zn to hetaerolite. Linear combination fitting of Zn EXAFS was conducted using hetaerolite and Zn-coprecipitated birnessite as end members, and the results are shown in Fig. 6 and Table S1. The fitting results suggested a very fast transformation, with more than 60% of the adsorbed Zn precipitated in hetaerolite within the first 3 h. This is consistent with the strong Mn (III)-removal ability of hetaerolite as discussed above. In k space EXAFS spectra, the 3-hour sample already resembled the spectra of hetaerolite. This fast transformation also explains why no desorbed Zn was detected in the solution.

3.4.2. Effect of Zn coprecipitation on the formation of feitknechtite

"F" peaks in XRD (Fig. 2) and FT-IR (Fig. 4) spectra showed the gradual production then consumption of feitknechtite along the 18-day reaction time. The initial F peaks in XRD are stronger in Zn-coprecipitation system under both anoxic and oxic conditions, indicating that feitknechtite production is faster from Zn-coprecipitated birnessite than from pure birnessite. In contrast to our results, Lefkowitz and Elzinga (2015) conducted similar transformation study using Zn-sorbed birnessite and found decreased feitknechtite precipitation rate in their Zn-sorbed birnessite system. If there were no birnessite structure modification (e.g. Zn-sorption system), the presence of Zn can affect feitknechtite production under anoxic conditions in several ways. Firstly, Zn sorption on birnessite surfaces could suppress Mn(II) sorption on birnessite and subsequent electron transfer. In several previous studies, pre-sorbed metal cation on MnOx surface modified surface charge and blocked surface sites, preventing further reaction between birnessite and other species. Ni coprecipitation with birnessite was found to decrease Pb and Zn adsorption on birnessite (Yin et al., 2012). Adsorbed Zn on birnessite surface could slow down the oxidation of As(III) by birnessite (Power et al., 2005). In our parallel study, Zn coprecipitation with δ-MnO_2 also suppressed Cd sorption on δ-MnO_2 by neutralizing negative δ-MnO_2 surface charges and blocking vacancy sites (Zhao et al., 2018). Secondly, the fast precipitation of hetaerolite (within minutes) consumed the newly-produced Mn(III), acting as a stronger Mn(III) sink than feitknechtite. Based on these two factors discussed above, feitknechtite precipitation would not be favored in Zn-sorbed birnessite system (i.e. no structure change to birnessite itself). Therefore, the accelerated production of feitknechtite within the first 3 days in our Zn-coprecipitation systems is like due to the birnessite structural and morphological modification by Zn-coprecipitation (as discussed in Section 3.1). Zn coprecipitation resulted in reduced birnessite particle size and more exposed surface area, which possibly resulted in fast Mn (III) production from the reaction between Zn-coprecipitated birnessite and Mn(II). The accumulation of feitknechtite was thus more significant in the Zn-coprecipitation system, despite the competition with hetaerolite precipitation. Previous studies showed that cobalt coprecipitation with birnessite enhanced the oxidative capacity of birnessite toward As (III) (Yin et al., 2011), and cobalt coprecipitation with cryptomelane also enhanced Cr(III) oxidation (due to higher surface area and average oxidation state) (Li et al., 2015). In this study, Zn-coprecipitated birnessite exhibited enhanced uptake and oxidative capability toward Mn (II), suggesting the potential enhancement of oxidative capacity of the solid, which warrants further investigation.

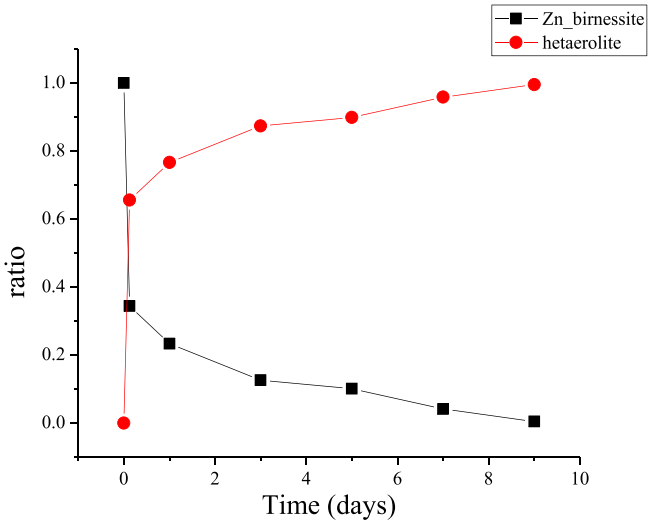

Fig. 6. Fractional composition of 0.2 cppt birnessite transformation products from linear combination fitting results of k^3-weighted Zn EXAFS.

Under oxic conditions, the faster feitknechtite formation in Zn-coprecipitation system could also result from a faster mineral surface-catalyzed Mn(II) oxidation by oxygen. Mn oxides have been widely used as effective catalysts and the catalytic reactivity is influenced by chemical composition and structure (Kim and Shim, 2010; Subbaraman et al., 2012; Kang et al., 2017). Metal impurity in Mn oxides (e.g. alkali (Kim and Shim, 2010; Kang et al., 2017), alkaline earth (Kim and Shim, 2010), and heavy metals (Yin et al., 2015b; Lin et al., 2001; Kang et al., 2006)) can generally enhance the catalytic capacity of Mn oxides. The mechanisms vary and are metal specific, such as expanded interlayer distance by alkali cations (Kang et al., 2017), increased surface area and average oxidations state by Fe (Yin et al., 2015b), and enhanced surface hydroxyl group by Co (Yin et al., 2011; Kim and Shim, 2010). In this study, the smaller particle size of the Zn-coprecipitated birnessite possibly enhanced the efficiency of the oxide for catalyzing Mn(II) oxidization by oxygen, contributing to the faster Mn(II) removal from solution and feitknechtite production under oxic condition.

3.4.3. Effect of Zn coprecipitation on the formation of manganite

"M" peaks in XRD data (Fig. 2) showed continuous transformation from feitknechtite to more stable manganite. This process did not change Mn(II) concentration under anoxic condition (Elzinga, 2011). Despite of modified kinetics of feitknechtite production and hetaerolite precipitation in Zn-coprecipitation system, Mn(II) concentration reached steady state at similar time (~5 days) as the pure birnessite system (Fig. 3A). This suggests that the precipitation of both feitknechtite and hetaerolite was almost finished after ~5 days. Linear combination fitting of Zn EXAFS data showed that ~90% of Zn precipitated as hetaerolite after 5 days, with continuous slow precipitation until almost 100% of Zn was precipitated as hetaerolite at ~day 9. The normalized FT-IR spectra of solids after 9 and 18-day transformation are shown in Fig. 4. Almost all feitknechtite was replaced by manganite

in the pure birnessite system after 9 days. With increasing Zn/Mn_{total} ratio from 0 to 0.2, the fraction of residual feitknechtite increased. After 18 days, manganite became the dominant phase in both pure and Zn-coprecipitation systems. However, there were still some remaining feitknechtite in the 0.2 cppt birnessite system, suggesting that increasing Zn content slowed down the transformation to manganite. This lower rate is likely due to the lower concentration of dissolved Mn(II) in the Zn-coprecipitation system (Fig. 3), which was previously shown to be proportional to manganite production rate (Elzinga, 2011).

Similar phenomena were also observed under oxic conditions where more feitknechtite remained in the 0.2 cppt birnessite system than in the pure birnessite system after 18 days. However, the dissolved Mn(II) concentration was almost the same in pure and Zn-coprecipitation systems from day 9 to 18, and this period was the primary time for feitknechtite transformation to tunnel structured manganite. Several factors might have contributed to the slow formation of manganite in Zn-coprecipitation system. Lefkowitz and Elzinga found that feitknechtite transformation was prohibited by adsorbed Ni (Lefkowitz and Elzinga, 2017). Metal cations such as Ni and Zn were also found to slow down the transformation of ferrihydrite to more stable phases (e.g. goethite and hematite) (Cornell, 1988; Ebinger and Schulze, 1990; Ford et al., 1999). These studies suggested that Fe/Mn (oxyhydr)oxide transformation were prohibited by the bonds between Fe/Mn and adsorbed metals (Lefkowitz and Elzinga, 2017; Ford et al., 1999; Giovanoli and Cornell, 1992). Similar mechanism might also preserved feitknechtite in this study. Secondly, Zn might block feitknechtite surface and compete with Mn(II) and interfere with the catalytic function of Mn(II) in feitknechtite transformation to manganite (Lefkowitz and Elzinga, 2017).

4. Conclusion and environmental implications

In this study, the effects of Zn coprecipitation on Mn(II)-induced birnessite transformation was explored. Zn-coprecipitated birnessite had smaller particle size compared to pure birnessite. During the interaction with Mn(II), compared to the pure birnessite system, a new Zn-containing mineral phase (hetaerolite) was formed in the Zn-coprecipitation system, modifying the transformation pathway and increasing Mn(II) removal and Mn(IV) consumption. Compared to Zn sorption on birnessite, the Zn coprecipitation system showed different transformation kinetics. Accelerated feitknechitite precipitation suggested enhanced redox and catalytic reactivity of Zn-coprecipitated birnessite. Compare to previous studies using pure MnOx, Zn-coprecipitation resulted in different phase (i.e. hetaerolite) with likely distinctive sorptive and oxidative properties and bioavailability.

Considering the common association of metal cations (e.g. Zn) with MnOx in natural environments, further investigations are warranted to explore the effects of metal-coprecipitation on MnOx structure modification and subsequent transformation kinetics and pathways, as well as the influence of other common environmental factors (e.g. oxygen level, pH, Mn(II) concentration) on the transformation process. Such information can help better constrain the roles of MnOx in the fate and transport of a range of nutrients and contaminants, as well as the Mn cycle itself. In addition, because MnOx are also widely used as oxidants and catalysts, the modified redox and/or catalytic property of metal-coprecipitated MnOx can provide information on the design and selection of targeting phases for environmental remediation and catalytic applications.

Acknowledgement

This research is supported by NASA under Grant #NNA15BB03A and NSF under Grant #1710285. We appreciate the support from beamline scientists Qing Ma (APS 5BM), Benjamin Reinhart, Sungsik Lee (APS 12BM), and Ryan Davis (SSRL 4-1). Portions of this research were conducted at the Advanced Photon Source (APS) and Stanford Synchrotron Radiation Lightsource (SSRL). APS is a U.S. Department of Energy (DOE) Office of Science User Facility operated by Argonne National Laboratory under Contract No. DE-AC02-06CH11357. Use of SSRL, SLAC National Accelerator Laboratory, is supported by DOE Office of Science, Office of Basic Energy Sciences under Contract No. DE-AC02-76SF00515.

Appendix A. Supplementary data

Details of reference compound XRD spectra; Mn XAS data of reference compounds and transformation products; Zn XAS LCF results; identification of transformation products using XRD and XAS; effects of light on the transformation process. Supplementary data to this article can be found online at https://doi.org/10.1016/j.chemgeo.2018.05.031.

References

Bargar, J.R., Tebo, B.M., Bergmann, U., Webb, S.M., Glatzel, P., Chiu, V.Q., Villalobos, M., 2005. Biotic and abiotic products of Mn (II) oxidation by spores of the marine *Bacillus* sp. strain SG-1. Am. Mineral. 90 (1), 143–154.

Bargar, J.R., Fuller, C.C., Marcus, M.A., Brearley, A.J., De la Rosa, M.P., Webb, S.M., Caldwell, W.A., 2009. Structural characterization of terrestrial microbial Mn oxides from Pinal Creek, AZ. Geochim. Cosmochim. Acta 73 (4), 889–910.

Bodeï, S., Manceau, A., Geoffroy, N., Baronnet, A., Buatier, M., 2007. Formation of todorokite from vernadite in Ni-rich hemipelagic sediments. Geochim. Cosmochim. Acta 71 (23), 5698–5716.

Chang, J., Tani, Y., Naitou, H., Miyata, N., Tojo, F., Seyama, H., 2014. Zn (II) sequestration by fungal biogenic manganese oxide through enzymatic and abiotic processes. Chem. Geol. 383, 155–163.

Cornell, R., 1988. The influence of some divalent cations on the transformation of ferrihydrite to more crystalline products. Clay Miner. 23 (3), 329–332.

Ebinger, M., Schulze, D., 1990. The influence of pH on the synthesis of mixed Fe-Mn oxide minerals. Clay Miner. 25 (4), 507–518.

Elzinga, E.J., 2011. Reductive transformation of birnessite by aqueous Mn (II). Environ. Sci. Technol. 45 (15), 6366–6372.

Elzinga, E.J., Kustka, A.B., 2015. A Mn-54 radiotracer study of Mn isotope solid–liquid exchange during reductive transformation of vernadite (δ-MnO_2) by aqueous Mn (II). Environ. Sci. Technol. 49 (7), 4310–4316.

Ford, R.G., Kemner, K., Bertsch, P.M., 1999. Influence of sorbate-sorbent interactions on the crystallization kinetics of nickel-and lead-ferrihydrite coprecipitates. Geochim. Cosmochim. Acta 63 (1), 39–48.

Giovanoli, R., Cornell, R.M., 1992. Crystallization of metal substituted ferrihydrites. J. Plant Nutr. Soil Sci. 155 (5), 455–460.

Grangeon, S., Manceau, A., Guilhermet, J., Gaillot, A.-C., Lanson, M., Lanson, B., 2012. Zn sorption modifies dynamically the layer and interlayer structure of vernadite. Geochim. Cosmochim. Acta 85, 302–313.

Hinkle, M.A.G., Dye, K.G., Catalano, J.G., 2017. Impact of Mn(II)-Manganese Oxide Reactions on Ni and Zn Speciation. Environ. Sci. Technol. 51 (6), 3187–3196. http://dx.doi.org/10.1021/acs.est.6b04347.

Jung, H., Chadha, T.S., Min, Y., Biswas, P., Jun, Y.-S., 2017a. Photochemically-assisted synthesis of birnessite nanosheets and their structural alteration in the presence of pyrophosphate. ACS Sustain. Chem. Eng. 5 (11), 10624–10632.

Jung, H., Chadha, T.S., Kim, D., Biswas, P., Jun, Y.-S., 2017b. Photochemically assisted fast abiotic oxidation of manganese and formation of δ-MnO_2 nanosheets in nitrate solution. Chem. Commun. 53 (32), 4445–4448.

Kang, M., Park, E.D., Kim, J.M., Yie, J.E., 2006. Cu–Mn mixed oxides for low temperature NO reduction with NH_3. Catal. Today 111 (3), 236–241.

Kang, Q., Vernisse, L., Remsing, R.C., Thenuwara, A.C., Shumlas, S.L., Mckendry, I.G., Klein, M.L., Borguet, E., Zdilla, M.J., Strongin, D.R., 2017. Effect of interlayer spacing on the activity of layered manganese oxide bilayer catalysts for the oxygen evolution reaction. J. Am. Chem. Soc. 139 (5), 1863–1870.

Kim, S.C., Shim, W.G., 2010. Catalytic combustion of VOCs over a series of manganese oxide catalysts. Appl. Catal. B Environ. 98 (3), 180–185.

Kwon, K.D., Refson, K., Sposito, G., 2013. Understanding the trends in transition metal sorption by vacancy sites in birnessite. Geochim. Cosmochim. Acta 101, 222–232.

Landrot, G., Ginder-Vogel, M., Livi, K., Fitts, J.P., Sparks, D.L., 2012. Chromium(III) oxidation by three poorly-crystalline manganese(IV) oxides. 1. Chromium(III)-oxidizing capacity. Environ. Sci. Technol. 46 (21), 11594–11600.

Lanson, B., Drits, V.A., Gaillot, A.-C., Silvester, E., Plançon, A., Manceau, A., 2002. Structure of heavy-metal sorbed birnessite: part 1. Results from X-ray diffraction. Am. Mineral. 87 (11 − 12), 1631–1645.

Lanson, B., Marcus, M.A., Fakra, S., Panfili, F., Geoffroy, N., Manceau, A., 2008. Formation of Zn–Ca phyllomanganate nanoparticles in grass roots. Geochim. Cosmochim. Acta 72 (10), 2478–2490.

Learman, D.R., Voelker, B.M., Vazquez-Rodriguez, A.I., Hansel, C.M., 2011. Formation of manganese oxides by bacterially generated superoxide. Nat. Geosci. 4 (2), 95–98.

Lefkowitz, J.P., Elzinga, E.J., 2015. Impacts of aqueous Mn (II) on the sorption of Zn (II) by hexagonal birnessite. Environ. Sci. Technol. 49 (8), 4886–4893.

Lefkowitz, J.P., Elzinga, E.J., 2017. Structural alteration of hexagonal birnessite by

aqueous Mn (II): impacts on Ni (II) sorption. Chem. Geol. 466, 524–532.
Lefkowitz, J.P., Rouff, A.A., Elzinga, E.J., 2013. Influence of pH on the reductive transformation of birnessite by aqueous Mn (II). Environ. Sci. Technol. 47 (18), 10364–10371.
Li, H., Liu, F., Zhu, M., Feng, X., Zhang, J., Yin, H., 2015. Structure and properties of co-doped cryptomelane and its enhanced removal of Pb^{2+} and Cr^{3+} from wastewater. J. Environ. Sci. 34, 77–85.
Lin, R., Liu, W.-P., Zhong, Y.-J., Luo, M.-F., 2001. Catalyst characterization and activity of Ag–Mn complex oxides. Appl. Catal. A Gen. 220 (1), 165–171.
Madison, A.S., Tebo, B.M., Luther, G.W., 2011. Simultaneous determination of soluble manganese (III), manganese (II) and total manganese in natural (pore) waters. Talanta 84 (2), 374–381.
Manceau, A., Lanson, B., Drits, V.A., 2002. Structure of heavy metal sorbed birnessite. Part III: results from powder and polarized extended X-ray absorption fine structure spectroscopy. Geochim. Cosmochim. Acta 66 (15), 2639–2663.
Mandernack, K.W., Post, J., Tebo, B.M., 1995. Manganese mineral formation by bacterial spores of the marine Bacillus, strain SG-1: evidence for the direct oxidation of Mn (II) to Mn (IV). Geochim. Cosmochim. Acta 59 (21), 4393–4408.
Murray, J.W., Dillard, J.G., Giovanoli, R., Moers, H., Stumm, W., 1985. Oxidation of Mn (II): initial mineralogy, oxidation state and ageing. Geochim. Cosmochim. Acta 49 (2), 463–470.
Murray, K.J., Webb, S.M., Bargar, J.R., Tebo, B.M., 2007. Indirect oxidation of Co(II) in the presence of the marine Mn(II)-oxidizing bacterium Bacillus sp. strain SG-1. Appl. Environ. Microbiol. 73 (21), 6905–6909.
Nico, P.S., Zasoski, R.J., 2000. Importance of Mn (III) availability on the rate of Cr (III) oxidation on δ-MnO_2. Environ. Sci. Technol. 34 (16), 3363–3367.
Post, J.E., 1999. Manganese oxide minerals: crystal structures and economic and environmental significance. Proc. Natl. Acad. Sci. 96 (7), 3447–3454.
Power, L.E., Arai, Y., Sparks, D.L., 2005. Zinc adsorption effects on arsenite oxidation kinetics at the birnessite-water interface. Environ. Sci. Technol. 39 (1), 181–187.
Ravel, B., Newville, M., 2005. ATHENA, ARTEMIS, HEPHAESTUS: data analysis for X-ray absorption spectroscopy using IFEFFIT. J. Synchrotron Radiat. 12 (4), 537–541.
Spiro, T.G., Bargar, J.R., Sposito, G., Tebo, B.M., 2009. Bacteriogenic manganese oxides. Acc. Chem. Res. 43 (1), 2–9.
Subbaraman, R., Tripkovic, D., Chang, K.-C., Strmcnik, D., Paulikas, A.P., Hirunsit, P., Chan, M., Greeley, J., Stamenkovic, V., Markovic, N.M., 2012. Trends in activity for the water electrolyser reactions on 3d M (Ni, Co, Fe, Mn) hydr (oxy) oxide catalysts. Nat. Mater. 11 (6), 550–557.
Tang, Y., Webb, S.M., Estes, E.R., Hansel, C.M., 2014. Chromium (III) oxidation by biogenic manganese oxides with varying structural ripening. Environ. Sci.: Processes Impacts 16 (9), 2127–2136.
Tebo, B.M., Bargar, J.R., Clement, B.G., Dick, G.J., Murray, K.J., Parker, D., Verity, R., Webb, S.M., 2004. Biogenic manganese oxides: properties and mechanisms of formation. Annu. Rev. Earth Planet. Sci. 32, 287–328.
Tu, S., Racz, G.J., Goh, T.B., 1994. Transformations of synthetic birnessite as affected by pH and manganese concentration. Clay Clay Miner. 42 (3), 321–330.
Villalobos, M., Toner, B., Bargar, J., Sposito, G., 2003. Characterization of the manganese oxide produced by *Pseudomonas putida* strain MnB1. Geochim. Cosmochim. Acta 67 (14), 2649–2662.
Villalobos, M., Escobar-Quiroz, I.N., Salazar-Camacho, C., 2014. The influence of particle size and structure on the sorption and oxidation behavior of birnessite: I. Adsorption of As(V) and oxidation of As(III). Geochim. Cosmochim. Acta 125, 564–581.
Wang, Y., Feng, X., Villalobos, M., Tan, W., Liu, F., 2012. Sorption behavior of heavy metals on birnessite: relationship with its Mn average oxidation state and implications for types of sorption sites. Chem. Geol. 292–293 (0), 25–34.
Webb, S., Tebo, B., Bargar, J., 2005. Structural characterization of biogenic Mn oxides produced in seawater by the marine *Bacillus* sp. strain SG-1. Am. Mineral. 90 (8–9), 1342–1357.
Yin, H., Feng, X., Qiu, G., Tan, W., Liu, F., 2011. Characterization of co-doped birnessites and application for removal of lead and arsenite. J. Hazard. Mater. 188 (1), 341–349.
Yin, H., Tan, W., Zheng, L., Cui, H., Qiu, G., Liu, F., Feng, X., 2012. Characterization of Ni-rich hexagonal birnessite and its geochemical effects on aqueous Pb^{2+}/Zn^{2+} and As (III). Geochim. Cosmochim. Acta 93, 47–62.
Yin, H., Liu, F., Feng, X., Hu, T., Zheng, L., Qiu, G., Koopal, L.K., Tan, W., 2013. Effects of Fe doping on the structures and properties of hexagonal birnessites–comparison with Co and Ni doping. Geochim. Cosmochim. Acta 117, 1–15.
Yin, H., Li, H., Wang, Y., Ginder-Vogel, M., Qiu, G., Feng, X., Zheng, L., Liu, F., 2014. Effects of Co and Ni co-doping on the structure and reactivity of hexagonal birnessite. Chem. Geol. 381, 10–20.
Yin, H., Liu, Y., Koopal, L.K., Feng, X., Chu, S., Zhu, M., Liu, F., 2015a. High co-doping promotes the transition of birnessite layer symmetry from orthogonal to hexagonal. Chem. Geol. 410, 12–20.
Yin, H., Dai, X., Zhu, M., Li, F., Feng, X., Liu, F., 2015b. Fe-doped cryptomelane synthesized by refluxing at atmosphere: structure, properties and photocatalytic degradation of phenol. J. Hazard. Mater. 296, 221–229.
Yu, Q., Sasaki, K., Tanaka, K., Ohnuki, T., Hirajima, T., 2013. Zinc sorption during bio-oxidation and precipitation of manganese modifies the layer stacking of biogenic birnessite. Geomicrobiol J. 30 (9), 829–839.
Zhao, H., Zhu, M., Li, W., Elzinga, E.J., Villalobos, M., Liu, F., Zhang, J., Feng, X., Sparks, D.L., 2016. Redox Reactions between Mn(II) and Hexagonal Birnessite Change Its Layer Symmetry. Environ. Sci. Technol. 50 (4), 1750–1758.
Zhao, S., Li, C., Liu, P., Huang, R., Saad, E.M., Tang, Y., 2018. Zinc presence during mineral formation affects the sorptive reactivity of manganese oxide. Soil Syst. 2 (2), 19.
Zhao, S., Wang, Q., Sun, J., Borkiewicz, O., Huang, R., Saad, E., Fields, B., Chen, S., Zhu, M., Tang, Y., 2018. Effect of Zn2+ presence during mineral formation on the structure of layered Mn oxides. Chem. Geol Revision submitted (2018/05/18).
Zhu, M., Paul, K.W., Kubicki, J.D., Sparks, D.L., 2009. Quantum chemical study of arsenic (III, V) adsorption on Mn-oxides: implications for arsenic (III) oxidation. Environ. Sci. Technol. 43 (17), 6655–6661.
Zhu, M., Ginder-Vogel, M., Parikh, S.J., Feng, X.-H., Sparks, D.L., 2010. Cation effects on the layer structure of biogenic Mn-oxides. Environ. Sci. Technol. 44 (12), 4465–4471.